Deng et al. Nanoscale Research Letters (2016) 11:29
DOI 10.1186/s11671-016-1246-7

Nanoscale Research Letters
a SpringerOpen Journal

NANO EXPRESS Open Access

One-Step Solvothermal Method to Prepare Ag/Cu_2O Composite With Enhanced Photocatalytic Properties

Xiaolong Deng, Chenggang Wang, E. Zhou, Jinzhao Huang, Minghui Shao, Xianqi Wei, Xiaojing Liu, Meng Ding* and Xijin Xu*

Abstract

Ag/Cu_2O microstructures with diverse morphologies have been successfully synthesized with different initial reagents of silver nitrate ($AgNO_3$) by a facile one-step solvothermal method. Their structural and morphological characteristics were carefully investigated by means of X-ray diffraction (XRD), scanning electron microscopy (SEM), and transmission electron microscopy (TEM), and the experimental results showed that the morphologies transformed from microcubes for pure Cu_2O to microspheres with rough surfaces for Ag/Cu_2O. The photocatalytic activities were evaluated by measuring the degradation of methyl orange (MO) aqueous solution under visible light irradiation. The photocatalytic efficiencies of MO firstly increased to a maximum and then decreased with the increased amount of $AgNO_3$. The experimental results revealed that the photocatalytic activities were significantly influenced by the amount of $AgNO_3$ during the preparation process. The possible reasons for the enhanced photocatalytic activities of the as-prepared Ag/Cu_2O composites were discussed.

Keywords: Ag/Cu_2O, Composites, Photocatalytic activity

Background

Over the past decades, the environmental problem, especially wastewater induced by organic dye pollutants, has become a fatal issue accompanying the rapid industry growth, which restricted the sustainable development of human beings [1–3]. Therefore, a great effort has been made for seeking the highly active photocatalysts which could be applied for the environmental remediation [4]. Recently, the hybrid structures, such as nanocomposites, which group the various materials with different properties together to offer the potential enhanced functions, have attracted much more attention [5, 6]. Metal-metal oxide semiconductor materials as one type of these hybrid structures have also been widely investigated due to their potential applications in the fields such as sensing [7, 8], antibacterial [5], charge-transfer process [9–11], optoelectronics [12, 13], energy storage [14], and catalysis [15, 16]. Additionally, it is believed that in the metal-semiconductor composites, metal deposits could act as the electron sinks which trap the photoinduced electrons transferring from the conduction band of semiconductor, while the photoinduced holes could remain on the semiconductor surface, and thus, the recombination of photoinduced electron-hole pairs could be prevented resulting in the improvement of photocatalytic efficiency [17, 18]. Among these metal-semiconductor hybrid structures, Ag/Cu_2O composites have been extensively explored based on the following reasons: (1) Ag, as one kind of relatively cheap noble metal, has also been investigated at nanoscale driven by its excellent sensing properties [19, 20], catalytic activities [21, 22], optical properties [23], thermal properties [24, 25], and inkjet ink particles [26]; (2) Cu_2O, as a typically low-cost and nontoxic p-type semiconductor, has a narrow direct bandgap of 2.0–2.2 eV, which could be used as photocatalysts under visible light [17, 27].

Cu_2O has been first investigated as a visible light-driven photocatalyst for water splitting since 1998 [28]. After that, many efforts have been made to improve the photocatalytic efficiency from the two aspects:

* Correspondence: sps_dingm@ujn.edu.cn; sps_xuxj@ujn.edu.cn
School of Physics and Technology, University of Jinan, 336 Nanxin Zhuang West Road, Jinan 250022, Shandong Province, People's Republic of China

(1) modulating the growth process to control the chemical stability, size, morphology, and architecture of Cu_2O [29–34]; (2) hindering the recombination of photogenerated electron-hole pairs [35] and photocorrosion [36, 37]. For Cu_2O-based photocatalysts, some actions, such as element doping [38–40] and heterojunction forming [41, 42], have been taken to enhance the photocatalytic activity compared with pure Cu_2O. Moreover, forming composite was also a very important approach to promote the photocatalytic efficiency for Cu_2O-based material [43, 44]. As mentioned above, Ag/Cu_2O, as an important composite, has also been considered a way to enhance the photocatalytic activity of Cu_2O [16–18, 27, 45]. Generally, Ag could be synthesized by various methods to form different morphologies, such as electrolysis method [46], biological method [47], reducing method [16], photocatalytic process [18], soaking method [27], and polyol process [45]. Likewise, there were many approaches to fabricate controllable Cu_2O structures, including hydrothermal method [45], solvothermal method [40], solution method [6, 16–18], and electrodeposition method [14, 27]. However, there are only a few reports to investigate the effect of Ag content on the photocatalytic efficiency of Ag/Cu_2O nanocomposites prepared by electron beam irradiation method [48]. So far, little information is available on the Ag content effect for photocatalytic properties of Ag/Cu_2O synthesized by a facile one-step solvothermal method.

In this work, a series of Ag/Cu_2O microstructures were fabricated by a facile solvothermal method by adding different amounts of silver nitrate ($AgNO_3$). The effect of Ag content on structures and morphologies of the as-synthesized Ag/Cu_2O composites were systematically investigated. Furthermore, the photocatalytic activities of Ag/Cu_2O composites prepared with different amounts of $AgNO_3$ for methyl orange (MO) dye in aqueous solution were performed. The results revealed that the photocatalytic activities of the as-prepared samples showed the maximal efficiency on degradation of MO related to the suitable amount of $AgNO_3$. The possible reasons for enhanced photocatalytic activities of the as-prepared Ag/Cu_2O composites were proposed.

Methods

Synthesis

All the chemical reagents, such as copper (II) nitrate trihydrate ($Cu(NO_3)_2{\cdot}3H_2O$), $AgNO_3$, ethylene glycol (EG), and MO, purchased from Sinopharm Chemical Reagent Co., Ltd. (SCRC; China), were of analytical grade and used without further purification. Typically, the samples were prepared as follows, similar to the previous report [40, 49]: 4 mmol $Cu(NO_3)_2{\cdot}3H_2O$ and certain amount of $AgNO_3$ were dissolved into 80 mL ethylene glycol followed by vigorous stirring to form a homogeneous solution. The mixture was then transferred into 100 mL Teflon-lined stainless steel autoclave. Thereafter, the sealed autoclave was kept at 140 °C for 10 h, followed by cooling down to room temperature naturally. The as-prepared precipitants were collected by centrifugation and washing with deionized water and ethanol several times. Finally, the products were obtained by drying the precipitants at 60 °C for 12 h in a vacuum oven. The samples were named as CA-0, CA-0.2, CA-0.5, CA-1, and CA-2 for the $AgNO_3$ amounts of 0, 0.2, 0.5, 1, and 2 mmol, respectively.

Characterization

X-ray powder diffraction (XRD) patterns of the as-prepared samples were analyzed by a German X-ray diffractometer (D8-Advance, Bruker AXS, Inc., Madison, WI, USA) equipped with Cu $K\alpha$ radiation ($\lambda = 0.15406$ nm). The morphologies of the as-synthesized products were observed by a field emission scanning electron microscope (FESEM; FEI Quanta FEG250, FEI, Hillsboro, USA) and transmission electron microscopy (TEM; JEOL-200CX, JEOL, Tokyo, Japan). X-ray photoelectron spectroscopy (XPS) was performed on a Thermo ESCALAB 250XI electron spectrometer equipped with Al $K\alpha$ X-ray radiation ($h\nu = 1486.6$ eV) as the source for excitation. The Brunauer-Emmett-Teller (BET) specific surface areas of the products were investigated by N_2 adsorption isotherm at 77 K using a specific surface area analyzer (QUADRASORB SI, Quantachrome Instruments, South San Francisco, CA, USA).

Photocatalytic Test

The photocatalytic activities of the as-prepared Ag/Cu_2O samples were performed by a UV-vis spectrophotometer (TU-1901, Beijing Purkinje General Instrument Co., Ltd, Beijing, China) at room temperature in air under visible light irradiation, which was similar to the previous reports [40, 49]. The visible light was generated by a 500-W Xe lamp equipped with a cut-off filter to remove the UV part with wavelength below 420 nm. In brief, a suspension was formed by dispersing 30 mg of powder into 50 mL of 20 mg/L MO aqueous solution. After that, the suspension was kept in dark for 30 min with stirring to reach the adsorption-desorption equilibrium of MO on the surface of Ag/Cu_2O samples. Ca. 3 mL suspension was taken out after a given irradiation time interval and centrifuged to filtrate the sample powders for the following UV-vis spectra test. The concentration of MO was characterized by measuring the absorbance properties

at 464 nm in UV-vis spectra to illuminate the photocatalytic activities.

Results and Discussion

Structural and Morphological Characterization of Samples

The structural properties of the as-synthesized Ag/Cu_2O composites are characterized as shown in Fig. 1. The peaks marked with "Δ" and "#" correspond to Cu_2O and Ag phases, respectively. The XRD pattern of sample CA-0 could be perfectly indexed into cubic Cu_2O (Joint Committee on Powder Diffraction Standards (JCPDS) no. 78-2076). There are no other characteristic peaks in sample CA-0, which demonstrate the pure phase of CA-0 with a cubic symmetry. However, for other samples (CA-0.2, CA-0.5, CA-1, and CA-2), the diffraction peaks illustrate the existence of both Cu_2O and Ag in Fig. 1. Furthermore, Cu phases (JCPDS no. 85-1326) are presented in the samples CA-0.5 and CA-1. It is found that the intensity of the diffraction peaks corresponding to Ag phases are enhanced, while that of Cu_2O phases are inhibited with the increase of $AgNO_3$ amounts, which confirm the dominant phase in the Ag/Cu_2O composites' change from Cu_2O to Ag.

The morphologies with different amounts of $AgNO_3$ are shown in Fig. 2. For CA-0, the hierarchical structure was mostly composed of regular cubic particles with size of about 500 nm, as shown in Fig. 2a, as well as a few spherical particles, as shown in Fig. 2b. Once $AgNO_3$ was added in the preparing process, the morphologies of the final products were almost entirely transformed into spheres with relatively smooth surface for CA-0.2 sample (Fig. 2c), besides some rough spheres consisting of pyramid particles. Figure 2d displays the as-grown sample CA-0.5 which was composed of nonuniform spheres with the diameter of 500–3500 nm, as well as some irregular structures. For samples CA-1 and CA-2, the SEM images (Fig. 2e, f) show the rough surface of spheres with relatively homogeneous diameter dispersion, while some cubic structures were also observed in sample CA-1. Typically, Fig. 3a shows the large-area (several tens micrometers) SEM image of the as-prepared CA-0.5 sample with spherical structures, and the corresponding energy dispersive X-ray spectroscopy (EDS) elemental mappings in Fig. 3b–c shows that the distributions of Cu, O, and Ag elements shown in Fig. 3d are approximately homogeneous even in the large area.

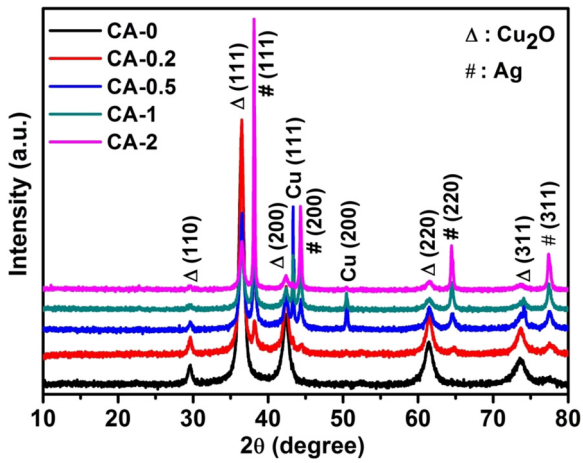

Fig. 1 XRD patterns of the as-prepared Ag/Cu_2O composites with different amounts of $AgNO_3$ (CA-0 0 mmol, CA-0.2 0.2 mmol, CA-0.5 0.5 mmol, CA-1 1 mmol, CA-2 2 mmol)

TEM observations as shown in Fig. 4 for the as-prepared Ag/Cu_2O samples further corroborate the observed morphologies with SEM. TEM images of sample CA-0 (Fig. 4a, b) depict cubic and spherical particles with size of about 520 nm and 1–2 μm, respectively, consistent with SEM observation. The spheres with homogeneous size distribution of about 1.8 μm are also observed in Fig. 4c for sample CA-0.2. Meanwhile, there are some hollow spheres with the diameter of 550 nm, agreeing with the SEM image. The spheres with heterogeneous diameter and irregular structures for CA-0.5 (Fig. 4d, e) are exhibited, as well as the spheres with uniform diameter and regular structures for CA-2 (Fig. 4f) confirmed the results of SEM observations.

The XPS spectra of the as-prepared samples CA-0, CA-0.5, and CA-2 are depicted in Fig. 5 to further confirm the composition and the elemental states in Ag/Cu_2O composites. The binding energies are calibrated by C 1s (284.8 eV). All the detected peaks on the survey scan spectra can be ascribed to C, O, and Cu elements for all samples, and Ag peaks are only found in Fig. 5b, c, which is consistent with the previous reports [17, 50]. No other elements' peaks were observed. C peaks mainly resulted from the hydrocarbon from the XPS instrument itself [50]. From the high-resolution XPS spectrum in the Cu $2p_{3/2}$ and Cu $2p_{1/2}$ binding energy region, the two main peaks locating at about 932.5 and 952.3 eV were in agreement with the reported value of Cu_2O [17, 40, 50, 51], respectively, which confirms the main composition of the structure is Cu_2O. In addition, the peaks locating at 944.1 and 962.7 eV in the Cu 2p region for CA-0.5 in Fig. 5b may be attributed to CuO due to the open $3d^9$ shell of Cu^{2+} [17, 48, 51]. The O 1s region shown in Fig. 5 could be fit into two main peaks locating at 530.4 and 531.6 eV (or 531.4 eV), which were ascribed to lattice oxygen of Cu_2O and surface-absorbed oxygen species [17, 40, 48, 50]. Furthermore, a peak at 532.5 eV was observed in the O 1s region shown in Fig. 5b, which originated from the

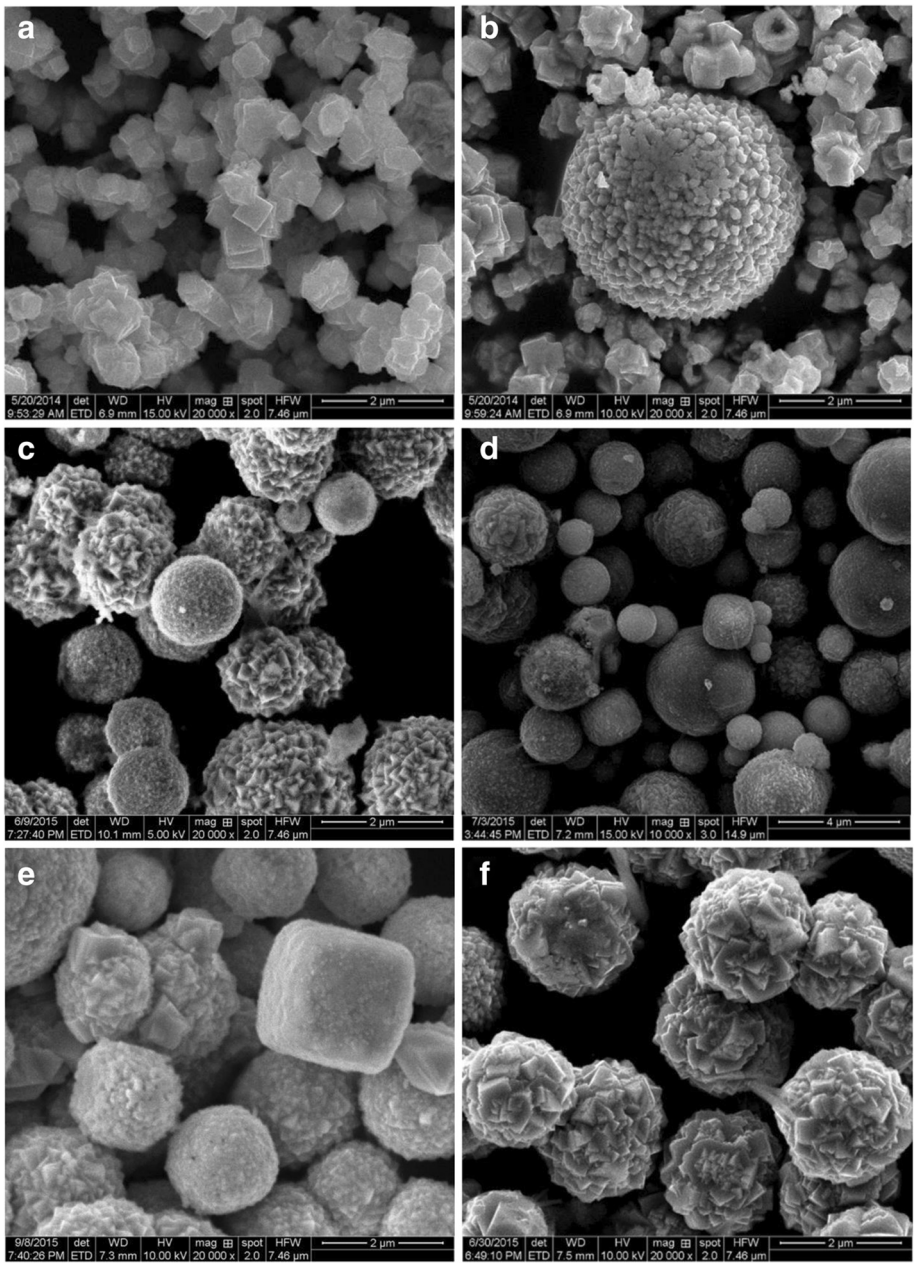

Fig. 2 SEM images of the as-grown samples with different amounts of $AgNO_3$ during the preparing process: **a**, **b** CA-0, **c** CA-0.2, **d** CA-0.5, **e** CA-1, and **f** CA-2

lattice oxygen of CuO [48]. Combining the peaks at 944.1 and 962.7 eV in the Cu 2p region with 532.5 eV in the O 1s region shown in Fig. 5b, it suggests that the existence of thin layer CuO forms on the surface of the sample (CA-0.5) [17]. The Ag 3d XPS spectra show no peaks for sample CA-0 as shown in Fig. 5a, which demonstrates the absence of Ag. However, there are two peaks locating at 368.3 and 374.3 eV shown in Fig. 5b, c in the Ag 3d region, which could be attributed to Ag $3d_{5/2}$ and Ag $3d_{3/2}$, respectively, matching well with the reported values of metallic Ag, indicating the existence of Ag with metallic nature [5, 48, 50]. No CuO could be detected from the XRD pattern, which indicates that the trace amount of CuO is present only on the surface of Ag/Cu_2O composites for sample CA-0.5 [17, 48].

Based on the above results, the synthesis mechanism for Ag/Cu_2O composites could be proposed as the following,

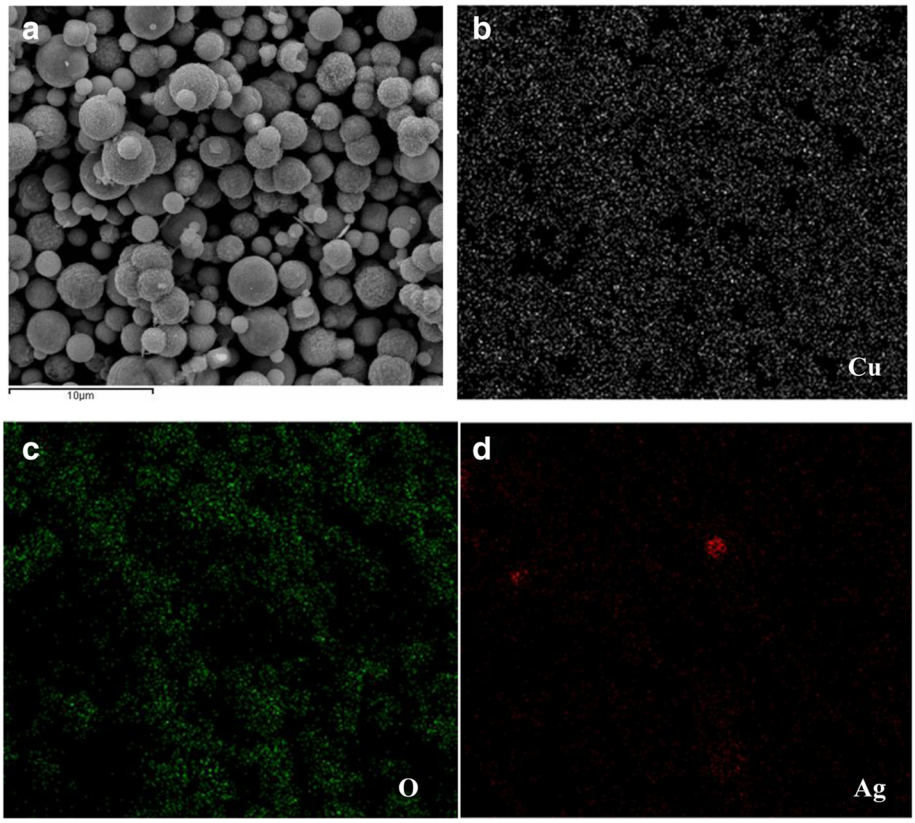

Fig. 3 Typically elemental mapping images of CA-0.5 sample. **a** The corresponding SEM image of the mapping area, **b** Cu mapping, **c** O mapping, and **d** Ag mapping

which is similar to the previous reports [5, 27, 40, 49, 50]. The possible chemical reactions should be as follows:

$$OHCH_2CH_2OH \rightarrow CH_3CHO + H_2O \quad (1)$$

$$OH{-}CH_2{-}CH_2{-}OH + Cu^{2+} \rightarrow [Cu(C_2H_6O)]^{2+} \quad (2)$$

$$[Cu(C_2H_6O)]^{2+} + H_2O \rightarrow Cu(OH)_2 + HOCH_2CH_2OH + 2H^+ \quad (3)$$

$$2Cu(OH)_2 + 2CH_3CHO \rightarrow Cu_2O + CH_3{-}CO{-}CO{-}CH_3 + 3H_2O \quad (4)$$

$$Cu(OH)_2 + CH_3CHO \rightarrow Cu + CH_3COOH + H_2O \quad (5)$$

$$2Cu + 4CH_3COOH + O_2 \rightarrow 2Cu(CH_3COO)_2 + 2H_2O \quad (6)$$

The reactions (Eqs. 5 and 6) sufficiently occurred in this work, and finally only Cu_2O existed in the products due to long reaction time [40, 49]. For sample CA-0, there is no addition of $AgNO_3$ resulting in the final product of Cu_2O. Once $AgNO_3$ was added into the solution, the following chemical reactions could occur according to the previous reports [27, 50, 52–54]:

$$2Ag^+ + 2CH_3CHO \rightarrow 2Ag + CH_3CO{-}COCH_3 + 2H^+ \quad (7)$$

$$2Ag^+ + Cu_2O + 2H^+ \rightarrow 2Cu^{2+} + 2Ag + H_2O \quad (8)$$

$$2Ag^+ + Cu_2O + H_2O \rightarrow 2Cu^{2+} + 2Ag + 2OH^- \quad (9)$$

$$Ag^+ + Cu \rightarrow Cu^{2+} + Ag \quad (10)$$

Therefore, the formed Cu^{2+} species may be absorbed on the surface of Cu_2O to form CuO for some samples such as CA-0.5 [27]. Meanwhile, the formation of Ag covered on Cu_2O to prevent the further reaction to some extent [27]. Nevertheless, metallic Cu could also be observed in some samples depending on the amount of $AgNO_3$. The reason was ascribed to be the broken equilibrium because of the additional reaction of Eq. 10 occurring [54]. When the amount of $AgNO_3$ (CA-0.2) was little, the reaction system was no significant difference from that of preparing sample CA-0. Therefore, almost no metallic Cu was observed in this sample (CA-0.2). Once the amount of $AgNO_3$ was sufficiently

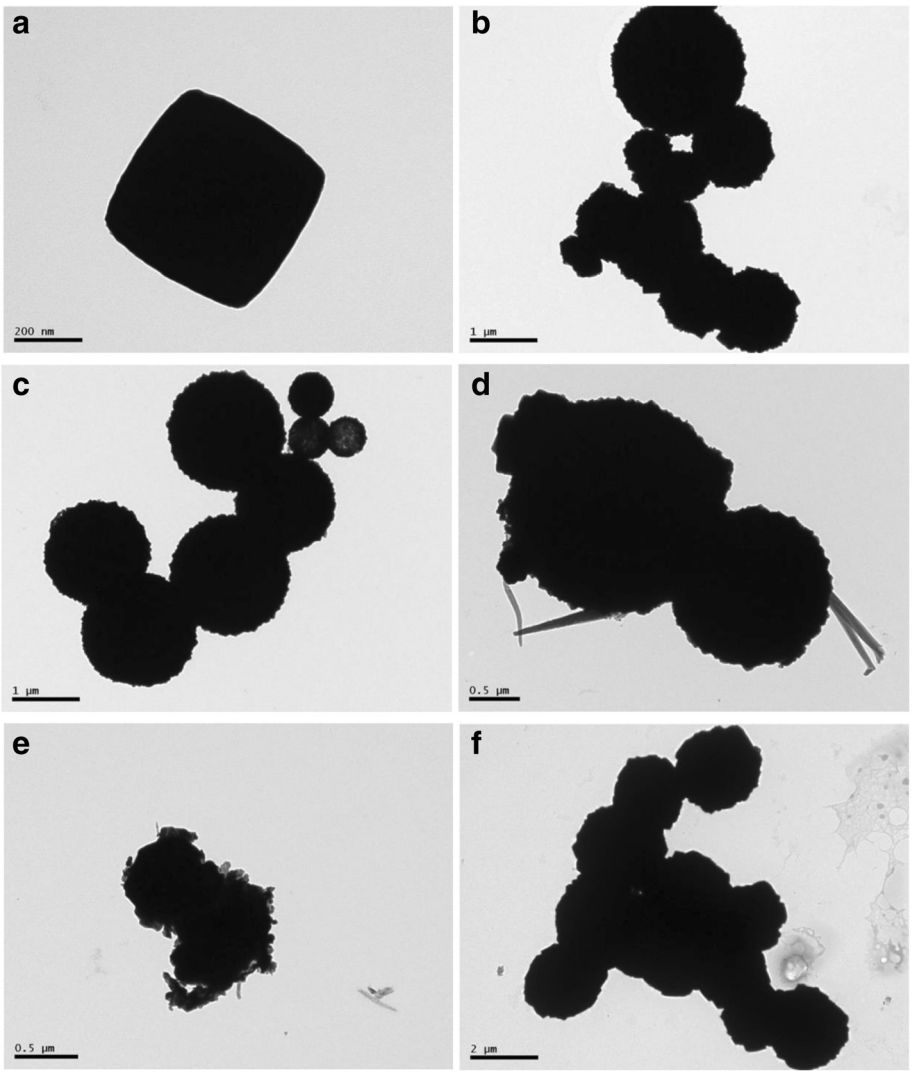

Fig. 4 Typical TEM images of the as-prepared Ag/Cu_2O samples. **a**, **b** CA-0; **c** CA-0.2; **d**, **e** CA-0.5; and **f** CA-2

enough (CA-2), there was also almost no existence of Cu due to the complete dissolution of Cu into Cu^{2+} according to Eq. 10. However, if the amount of $AgNO_3$ was not enough (CA-0.5 and CA-1), the reaction system equilibrium would be broken compared with the absence of $AgNO_3$ (CA-0), and Cu would be partly dissolved resulting in the residual of Cu. Thus, the Ag/Cu_2O composites were obtained when $AgNO_3$ was added during the fabrication process, which was confirmed by XRD patterns and XPS spectra.

Photocatalytic Activity of Samples

The photocatalytic activities of the as-prepared samples as photocatalysts on the degradation of MO were evaluated under visible light irradiation, as shown in Fig. 6. From Fig. 6a, it could be seen that the degradation efficiency of Ag/Cu_2O composite is higher than that of pure Cu_2O (CA-0) with the increment of $AgNO_3$ (CA-0.2 and CA-0.5). However, further increase of $AgNO_3$ amount resulted in the decrease of degradation efficiency (CA-1 and CA-2). For a detailed analysis of photocatalytic degradation kinetics of MO aqueous solution, the pseudo first-order model was applied to determine the rate constant of photodegradation with respect to the degradation time when the initial concentration of the pollutant is low, as expressed by Eq. 11 [3, 40, 49, 50].

$$\ln\left({}^{C}/_{C_0}\right) = -kt \tag{11}$$

where C_0 is the initial concentration of MO, C is the concentration at time t, and k is the reaction rate constant. The photocatalytic degradation kinetics of MO aqueous solution on the basis of the plots of

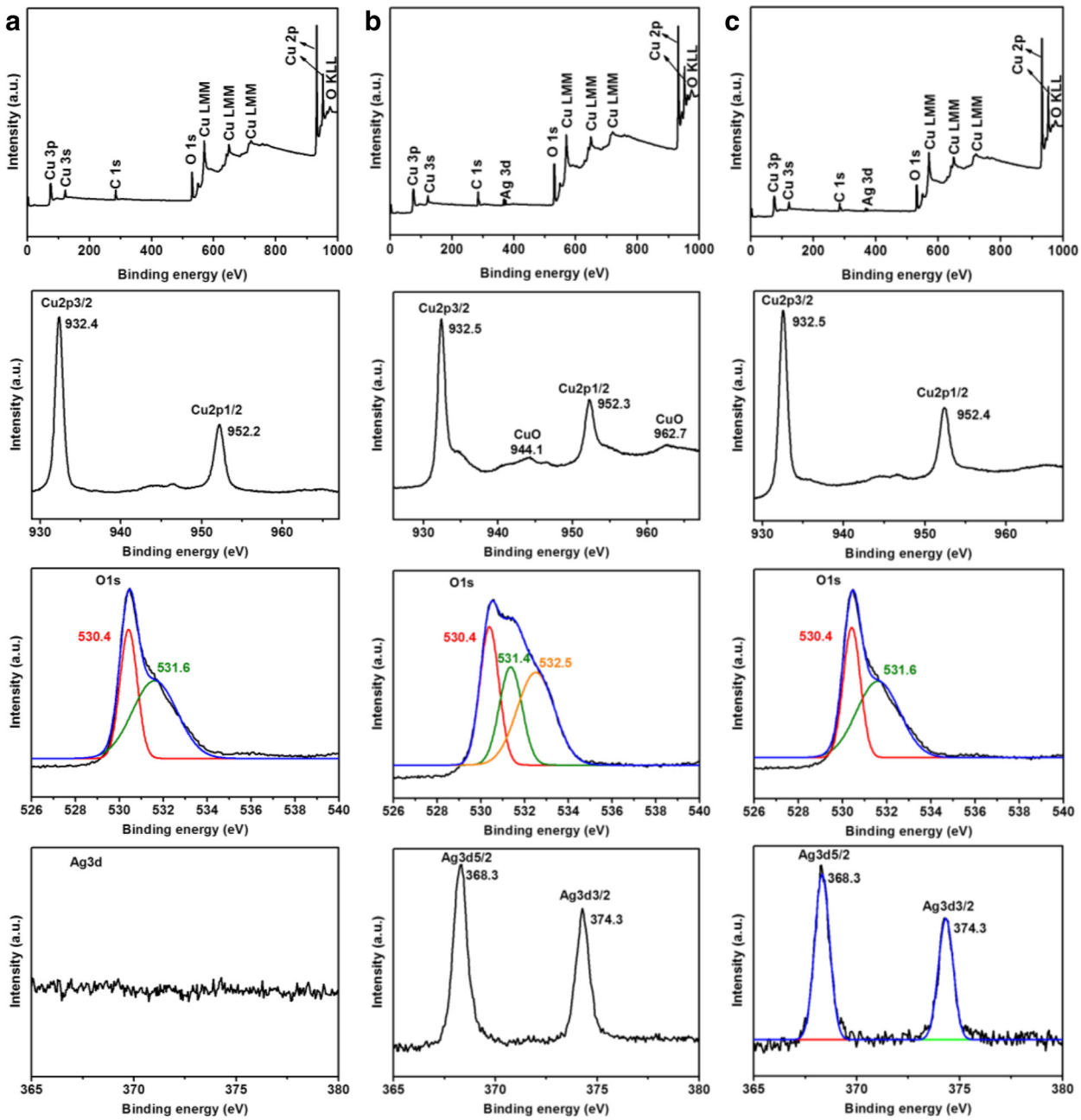

Fig. 5 Typical XPS spectrum of the as-grown Ag/Cu_2O samples including XPS full spectrum, Cu 2p spectrum, O 1s spectrum, and Ag 3d spectrum, respectively. **a** CA-0, **b** CA-0.5, and **c** CA-2

$\ln(C/C_0)$ versus time t was described in Fig. 6b. The rate constant (k) was given by the slopes of linear fit and estimated to be 0.02052, 0.03096, 0.05549, 0.01839, and 0.00729 min^{-1} for samples CA-0, CA-0.2, CA-0.5, CA-1, and CA-2, respectively. The rate constant values illustrated that the degradation rates for MO dye with the sequence of CA-0.5>CA-0.2>CA-0>CA-1>CA-2. For intuitive description of rate constant, the values were plotted versus the $AgNO_3$ content during the preparing process for Ag/Cu_2O samples, as illustrated in Fig. 7a. It showed more clearly that the rate constant achieved the maximum at the $AgNO_3$ content of 0.5 mmol (sample CA-0.5).

The causes for the vibration of photodegradation rates could be ascribed to as the following according to the literatures [17, 18, 27, 48, 50]: (1) surface plasmon resonance, which means that the photoexcited plasmonic energy in the Ag particles transferred into Cu_2O resulting in the more generation of electron-hole pairs in the

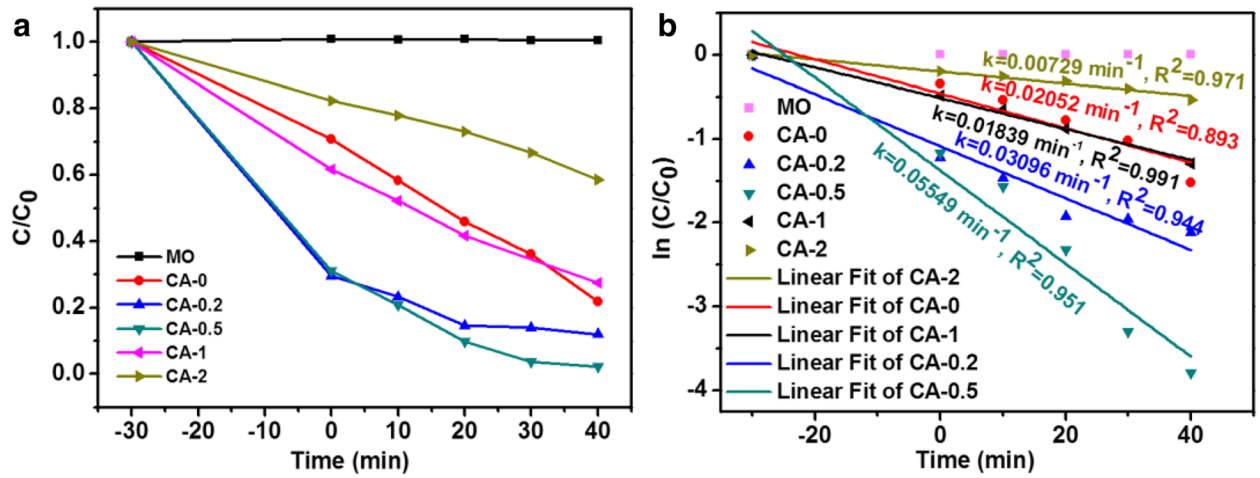

Fig. 6 **a** Relative concentration changes of MO as a function of irradiation time for Ag/Cu_2O samples under visible light irradiation. **b** Photocatalytic degradation kinetics of MO aqueous solution in the presence of Ag/Cu_2O samples

Cu_2O, which is beneficial to improve the photocatalytic activity; (2) Ag particles act as electron sinks, which means the photogenerated electrons transferring from the conduction band of Cu_2O to Ag particles, leading to the improvement in photocatalytic activity over an extended wavelength range and to prevent the recombination of photogenerated electron-hole pairs and enhance the interfacial charge-transfer and thus promotes the photocatalytic activity; (3) the enlarged specific surface area also improves the photocatalytic activity by increasing the contact area. However, with the increasement of the $AgNO_3$ content, the photocatalytic effect decreases. The specific surface areas of the as-prepared samples are described in Fig. 7b. The trend of specific surface area vibration was not consistent with the photodegradation rate, especially, for CA-0.5. The reason may be ascribed to the morphology transformation due to the addition of $AgNO_3$, which was in agreement with the SEM and TEM observations. The photodegradation activity vibration could be explained as follows: the excessive Ag causes the aggregation of Ag particles, resulting in the decrease of capturing the photogenerated electrons and the shield of the visible light absorption by Cu_2O, leading to the deterioration of photo-utilizing efficiency. In addition to the aforementioned reasons, the morphology was also one of the key factors for the photocatalytic activity. In this work, the morphology transformation experienced the following procedure: regular cube to smooth sphere to rough sphere with the increase of $AgNO_3$. The morphology would not only affect the specific surface area of the as-prepared samples as mentioned above but also influence the exposed crystal

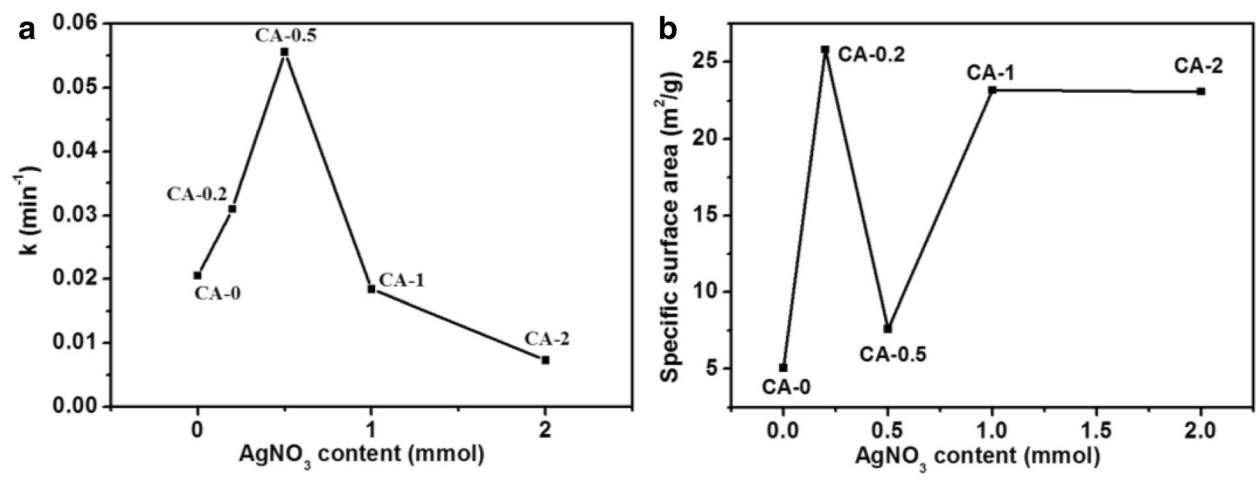

Fig. 7 Plots of **a** reaction rate constant and **b** specific surface area versus $AgNO_3$ content during the preparing process for Ag/Cu_2O samples

surfaces as previously reported [55, 56] which had significant impact on the photocatalytic activity. It is reported that [111] surfaces had much higher photocatalytic activity for Cu_2O and the cubic and spherical particles were mainly covered by [100] or [110] surfaces [55]. Combining SEM and TEM observations, the samples were reasonable to have the sequence of photocatalytic activities as shown in Fig. 7a (CA-0 (cube), CA-0.2 (spheres consisted of pyramid particles), CA-0.5 (spheres composed of pyramid particles and other irregular structures), CA-1 (cube and cube formed sphere), CA-2 (sphere composed of cubic particles)). Finally, Cu contained in some samples (CA-0.5 and CA-1) also contributed to the enhanced photocatalytic activities by promoting the rapid separation of photogenerated electrons and holes in the interfaces between Cu and Cu_2O [49, 57, 58]. However, the existence of Cu was not the dominant factor responsible for the enhanced photocatalytic activities by comparing the photodegradation rate of CA-1 with CA-0. In a word, the photocatalytic activity of Cu_2O on decomposition of MO dye in aqueous solution is enhanced by the formation of Ag particles with suitable amount of Ag content, which plays the dominant role, and the morphology effect.

The cycle runs in the photocatalytic degradation of MO aqueous solution in the presence of Ag/Cu_2O catalysts under visible light irradiation were investigated to evaluate the durability of Ag/Cu_2O composite for water treatment. All the experiments were carried out in the same conditions. Figure 8 presents the corresponding results. As observed, the MO degradation ratio has no significant difference after 3 cycles, indicating that the as-prepared Ag/Cu_2O composites exhibit good durability as photocatalysts for photodegradation of MO in aqueous solution.

The stability of Ag/Cu_2O composite on the photodegradation of MO aqueous solution was estimated by characterizing the samples after photocatalytic test. The XRD patterns of CA-0 and CA-0.5 after photodegradation was plotted as shown in Fig. 9, which demonstrated no difference from the initial states depicted in Fig. 1. The morphologies observed by SEM and TEM in Fig. 10 were almost no change compared with the corresponding samples before photodegradation measurement shown in Fig. 2. However, XPS spectra of CA-0.5 after photodegradation were different from the initial state while the spectra of CA-0 kept the same, as depicted in Fig. 11. The peaks denoted CuO in the XPS spectra of CA-0.5 disappeared in the Cu 2p and O 1s regions, which could be ascribed to the reduction of CuO to form Cu_2O induced by the photogenerated electrons [59]. Nevertheless, the XPS showed no change of the main component of Ag/Cu_2O composite for the sample CA-0.5 after photodegradation. Therefore, these results confirmed the stability of the as-prepared Ag/Cu_2O composites for the degradation of MO in aqueous solution under visible light irradiation.

Conclusions

In summary, Ag/Cu_2O composites were successfully synthesized by a facile one-step solvothermal method. The structural and morphological properties were characterized by XRD, SEM, TEM, and XPS, which demonstrated that the $AgNO_3$ amount during the fabrication process significantly affected the surface, size distribution, morphology, and specific surface area of the as-grown Ag/Cu_2O composites. The photocatalytic activities of the as-prepared Ag/Cu_2O composites on the photodegradation of MO dye were evaluated under visible light irradiation. The results illustrated that Ag

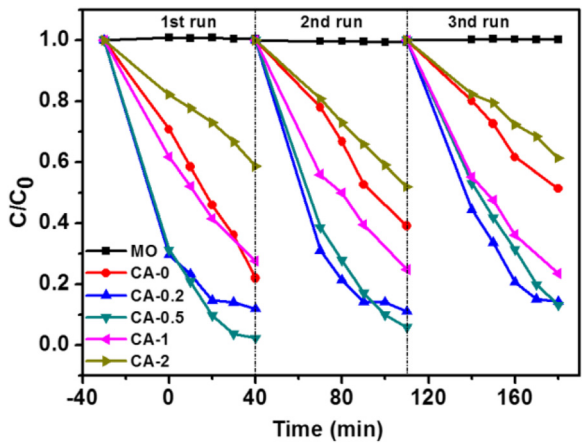

Fig. 8 Cycling runs in the photocatalytic degradation of MO aqueous solution in the presence of Ag/Cu_2O catalysts under visible light irradiation

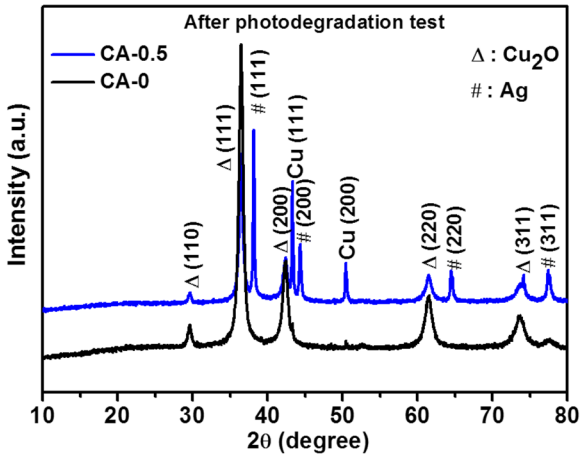

Fig. 9 XRD patterns of Ag/Cu_2O composites (CA-0 0 mmol and CA-0.5 0.5 mmol) after photodegradation measurement

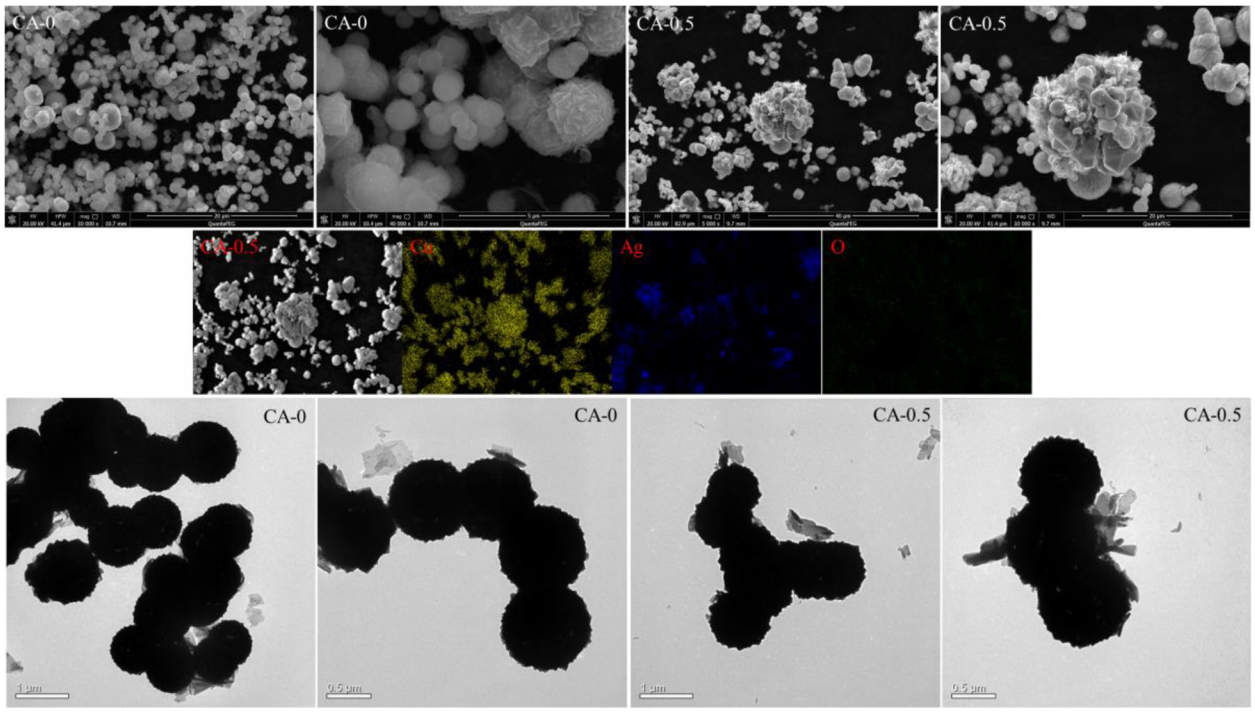

Fig. 10 SEM (*upper panel*), elemental mapping (*middle panel*), and TEM (*lower panel*) images of Ag/Cu_2O composites (CA-0 and CA-0.5) after photodegradation measurement

particles played an important role in the photodegradation of MO by surface plasmon resonance and acting as electron sinks. However, excessive Ag would decrease the photocatalytic activity because of shielding the visible light absorption by Cu_2O and lowering the capture of photogenerated electrons. The photodegradation of MO was also affected by the morphology of the as-prepared samples, though Ag particles were the dominant factor in this work. The as-prepared Ag/Cu_2O composites have good stabilities as photocatalysts for photodegradation of MO in aqueous solution, illustrating to be promising in wastewater treatment.

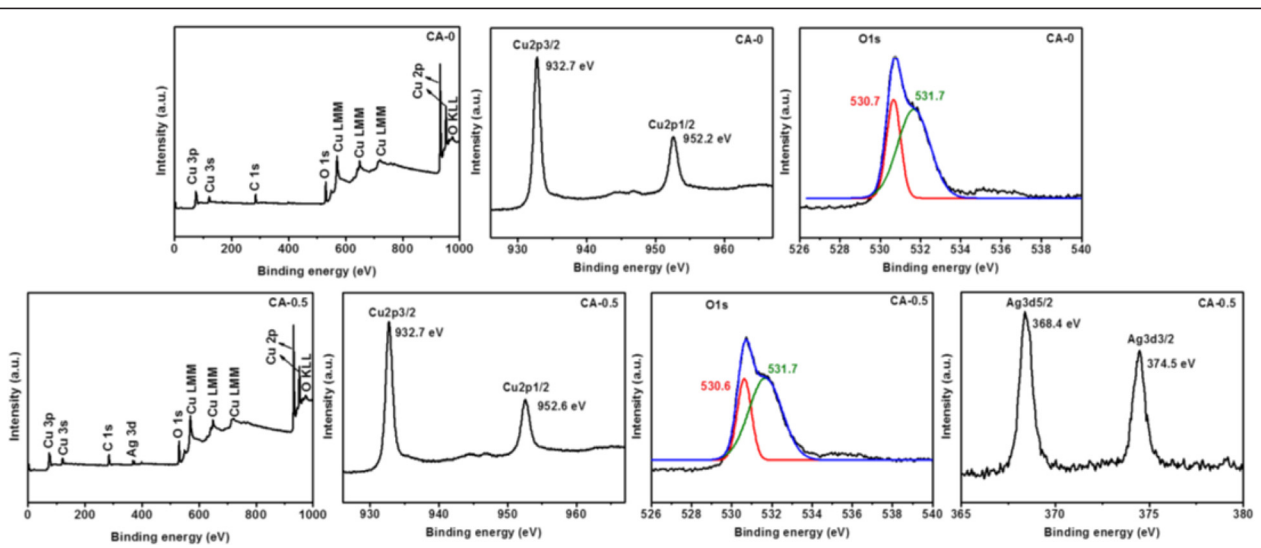

Fig. 11 The XPS spectrum of Ag/Cu_2O composites after photodegradation test including XPS full spectrum, Cu 2p spectrum, O 1s spectrum, and Ag 3d spectrum, respectively. (*Upper panel*) CA-0 and (*lower panel*) CA-0.5

Competing interests
The authors declare that they have no competing interests.

Authors' contributions
XLD, JZH, MHS, XQW, XJL, MD, and XJX planned the projects and designed the experiments; XLD, CGW, and EZ carried out the experiments; XLD, MD, and XJX analyzed the data and wrote the paper. All authors read and approved the final manuscript.

Acknowledgements
This work was supported by the Encouragement Foundation for Excellent Middle-Aged and Young Scientist of Shandong Province (Grant Nos. BS2014CL012 and BS2013CL020), National Natural Science Foundation of China (Grant Nos. 21505050, 11304120, 61504048, and 61575081), a Project of Shandong Province Higher Educational Science and Technology Program (Grant No. J15LJ06), and Shandong Provincial Natural Science Foundation (ZR2013AM008).

Received: 10 November 2015 Accepted: 6 January 2016
Published online: 19 January 2016

References

1. Li HJ, Zhou Y, Tu WG, Ye JH, Zou ZG (2015) State-of-the-art progress in diverse heterostructured photocatalysts toward promoting photocatalytic performance. Adv Funct Mater 25:998–1013
2. Han SC, Hu LF, Liang ZQ, Wageh S, Al-Ghamdi AA, Chen YS, Fang XS (2014) One-step hydrothermal synthesis of 2D hexagonal nanoplates of α-Fe_2O_3/graphene composites with enhanced photocatalytic activity. Adv Funct Mater 24:5719–5727
3. Liu L, Lin SL, Hu JS, Liang YH, Cui WQ (2015) Plasmon-enhanced photocatalytic properties of nano Ag@AgBr on single-crystalline octahedral Cu_2O (111) microcrystals composite photocatalyst. Appl Surf Sci 330:94–103
4. Dong F, Zhao ZW, Xiong T, Ni ZL, Zhang WD, Sun YJ, Ho WK (2013) In situ construction of g-C3N4/g-C3N4 metal-free heterojunction for enhanced visible-light photocatalysis. ACS Appl Mater Interfaces 5:11392–11401
5. Lu WW, Liu GS, Gao SY, Xing ST, Wang JJ (2008) Tyrosine-assisted preparation of Ag/ZnO nanocomposites with enhanced photocatalytic performance and synergistic antibacterial activities. Nanotechnology 19:445711
6. Kuo CH, Hua TE, Huang MH (2009) Au nanocrystal-directed growth of Au-Cu_2O core-shell heterostructures with precise morphological control. J Am Chem Soc 131:17871–17878
7. Rai P, Khan R, Raj S, Majhi SM, Park KK, Yu YT, Lee IH, Sekhar PK (2014) Au@Cu_2O core-shell nanoparticles as chemiresistors for gas sensor applications: effect of potential barrier modulation on the sensing performance. Nanoscale 6:581–588
8. Kim YS, Rai P, Yu YT (2013) Microwave assisted hydrothermal synthesis of Au@TiO_2 core-shell nanoparticles for high temperature CO sensing applications. Sens Actuators B 186:633–639
9. Kamat PV, Shanghavi B (1997) Interparticle electron transfer in metal/semiconductor composites. Picosecond dynamics of CdS-capped gold nanoclusters. J Phys Chem B 101:7675–7679
10. Kamat PV (2012) Manipulation of charge transfer across semiconductor interface. A criterion that cannot be ignored in photocatalyst design. J Phys Chem Lett 3:663–672
11. Wang YG, Yoon YH, Glezakou VA, Li J, Rousseau R (2013) The role of reducible oxide-metal cluster charge transfer in catalytic processes: new insights on the catalytic mechanism of CO oxidation on Au/TiO_2 from ab initio molecular dynamics. J Am Chem Soc 135:10673–10683
12. Mokari T, Sztrum CG, Salant A, Rabani E, Banin U (2005) Formation of asymmetric one-sided metal-tipped semiconductor nanocrystal dots and rods. Nat Mater 4:855–863
13. García de Arquer FP, Konstantatos G (2015) Metal-insulator-semiconductor heterostructures for plasmonic hot-carrier optoelectronics. Opt Express 23:14715–14723
14. Dong CQ, Wang Y, Xu JL, Cheng GH, Yang WF, Kou TY, Zhang ZH, Ding Y (2014) 3D binder-free Cu_2O@Cu nanoneedle arrays for high-performance asymmetric supercapacitors. J Mater Chem A 2:18229–18235
15. Wang X, Fan HQ, Ren PR (2013) Self-assemble flower-like SnO_2/Ag heterostructures: correlation among composition, structure and photocatalytic activity. Colloid Surface A: Physicochem Eng Aspects 419:140–146
16. Li JT, Cushing SK, Bright J, Meng FK, Senty TR, Zheng P, Bristow AD, Wu NQ (2013) Ag@Cu_2O core-shell nanoparticles as visible-light plasmonic photocatalysts. ACS Catal 3:47–51
17. Yang JB, Li Z, Zhao CX, Wang Y, Liu XQ (2014) Facile synthesis of Ag-Cu_2O composites with enhanced photocatalytic activity. Mater Res Bull 60:530–536
18. Wang ZH, Zhao SP, Zhu SY, Sun YL, Fang M (2011) Photocatalytic synthesis of M/Cu_2O (M = Ag, Au) heterogeneous nanocrystals and their photocatalytic properties. CrystEngComm 13:2262–2267
19. Mahmoud MA, El-Sayed MA (2013) Different plasmon sensing behavior of silver and gold nanorods. J Phys Chem Lett 4:1541–1545
20. Hou H, Wang P, Zhang J, Li CP, Jin YD (2015) Graphene oxide-supported Ag nanoplates as LSPR tunable and reproducible substrates for SERS applications with optimized sensitivity. ACS Appl Mater Interfaces 7:18038–18045
21. Roucoux A, Schulz J, Patin H (2002) Reduced transition metal colloids: a novel family of reusable catalysts? Chem Rev 102:3757–3778
22. Christopher P, Linic S (2010) Shape- and size-specific chemistry of Ag nanostructures in catalytic ethylene epoxidation. ChemCatChem 2:78–83
23. Wu J, Tan LH, Hwang K, Xing H, Wu PW, Li W, Lu Y (2014) DNA sequence-dependent morphological evolution of silver nanoparticles and their optical and hybridization properties. J Am Chem Soc 136:15195–15202
24. Xu XJ, Fei GT, Yu WH, Chen L, Zhang LD, Ju X, Hao XP, Wang BY (2006) In situ x-ray diffraction study of the thermal expansion of the ordered arrays of silver nanowires embedded in anodic alumina membranes. Appl Phys Lett 88:211902
25. Xu XJ, Fei GT, Yu WH, Zhang LD, Ju X, Hao XP, Wang DN, Wang BY (2006) In situ x-ray diffraction study of the size dependent thermal expansion of silver nanowires. Appl Phys Lett 89:181914
26. Lee CL, Chang KC, Syu CM (2011) Silver nanoplates as inkjet ink particles for metallization at a low baking temperature of 100 °C. Colloid Surface A: Physicochem Eng Aspects 381:85–91
27. Wei SQ, Shi J, Ren HJ, Li JQ, Shao ZC (2013) Fabrication of Ag/Cu_2O composite films with a facile method and their photocatalytic activity. J Mol Catal A Chem 378:109–114
28. Hara M, Kondo T, Komoda M, Ikeda S, Shinohara K, Tanaka A, Kondo JN, Domen K (1998) Cu_2O as a photocatalyst for overall water splitting under visible light irradiation. Chem Commun. doi:10.1039/A707440I
29. Kumar B, Saha S, Ganguly A, Ganguli AK (2014) A facile low temperature (350 °C) synthesis of Cu_2O nanoparticles and their electrocatalytic and photocatalytic properties. RSC Adv 4:12043–12049
30. Liu L, Qi YH, Hu JS, Liang YH, Cui WQ (2015) Efficient visible-light photocatalytic hydrogen evolution and enhanced photostability of core@shell Cu_2O@g-C_3N_4 octahedra. Appl Surf Sci 351:1146–1154
31. Zhai W, Sun FQ, Chen W, Zhang LH, Min ZL, Li WS (2013) Applications of Cu_2O octahedral particles on ITO glass in photocatalytic degradation of dye pollutants under a halogen tungsten lamp. Mater Res Bull 48:4953–4959
32. Li SK, Li CH, Huang FZ, Wang Y, Shen YH, Xie AJ, Wu Q (2011) One-pot synthesis of uniform hollow cuprous oxide spheres fabricated by single-crystalline particles via a simple solvothermal route. J Nanopart Res 13:2865–2874
33. Pan L, Zou JJ, Zhang TR, Wang SB, Li Z, Wang L, Zhang XW (2014) Cu_2O film via hydrothermal redox approach: morphology and photocatalytic performance. J Phys Chem C 118:16335–16343
34. Mao YC, He JT, Sun XF, Li W, Lu XH, Gan JY, Liu ZQ, Gong L, Chen J, Liu P, Tong YX (2012) Electrochemical synthesis of hierarchical Cu_2O stars with enhanced photoelectrochemical properties. Electrochim Acta 62:1–7
35. Zhang LS, Li JL, Chen ZG, Tang YW, Yu Y (2006) Preparation of Fenton reagent with H_2O_2 generated by solar light-illuminated nano-Cu_2O/MWNTs composites. Appl Catal A-Gen 299:292–297
36. Huang L, Peng F, Yu H, Wang HJ (2009) Preparation of cuprous oxides with different sizes and their behaviors of adsorption, visible-light driven photocatalysis and photocorrosion. Solid State Sci 11:129–138
37. Bessekhouad Y, Robert D, Weber JV (2005) Photocatalytic activity of Cu_2O/TiO_2, Bi_2O_3/TiO_2 and $ZnMn_2O_4/TiO_2$ heterojunctions. Catal Today 101:315–321
38. Heng BJ, Xiao T, Tao W, Hu XY, Chen XQ, Wang BX, Sun DM, Tang YW (2012) Zn doping-induced shape evolution of microcrystals: the case of cuprous oxide. Cryst Growth Des 12:3998–4005
39. Du YL, Zhang N, Wang CM (2010) Photo-catalytic degradation of trifluralin by SnO_2-doped Cu_2O crystals. Catal Commun 11:670–674

40. Deng XL, Zhang Q, Zhou E, Ji CJ, Huang JZ, Shao MH, Ding M, Xu XJ (2015) Morphology transformation of Cu_2O sub-microstructures by Sn doping for enhanced photocatalytic properties. J Alloy Comp 649:1124–1129
41. Tian QY, Wu W, Sun LL, Yang SL, Lei M, Zhou J, Liu Y, Xiao XH, Ren F, Jiang CZ, Roy VAL (2014) Tube-like ternary α-Fe_2O_3@SnO_2@Cu_2O sandwich heterostructures: synthesis and enhanced photocatalytic properties. ACS Appl Mater Inter 6:13088–13097
42. Liu LM, Yang WY, Sun WZ, Li Q, Shang JK (2015) Creation of Cu_2O@TiO_2 composite photocatalysts with p-n heterojunctions formed on exposed Cu_2O facets, their energy band alignment study, and their enhanced photocatalytic activity under illumination with visible light. ACS Appl Mater Inter 7:1465–1476
43. Yu HG, Yu JG, Liu SW, Mann S (2007) Template-free hydrothermal synthesis of CuO/Cu_2O composite hollow microspheres. Chem Mater 19:4327–4334
44. Zeng B, Chen XH, Luo YX, Liu QY, Zeng WJ (2014) Graphene spheres loaded urchin-like Cu_xO ($x = 1$ or 2) for use as a high performance photocatalyst. Ceram Int 40:5055–5059
45. Yang SY, Zhang SS, Wang HJ, Yu H, Fang YP, Peng F (2015) Controlled preparation of Ag-Cu_2O nanocorncobs and their enhanced photocatalytic activity under visible light. Mater Res Bull 70:296–302
46. Theivasanthi T, Alagar M (2012) Electrolytic synthesis and characterizations of silver nanopowder. Nano Biomed Eng 4:58–65
47. Varshney R, Bhadauria S, Gaur MS (2012) A review: biological synthesis of silver and copper nanoparticles. Nano Biomed Eng 4:99–106
48. Lin XF, Zhou RM, Zhang JQ, Fei ST (2009) A novel one-step electron beam irradiation method for synthesis of Ag/Cu_2O nanocomposites. Appl Surf Sci 256:889–893
49. Deng XL, Zhang Q, Zhao QQ, Ma LS, Ding M, Xu XJ (2015) Effects of architectures and H_2O_2 additions on the photocatalytic performance of hierarchical Cu_2O nanostructures. Nanoscale Res Lett 10:8
50. Zhang WX, Yang XN, Zhu Q, Wang K, Lu JB, Chen M, Yang ZH (2014) One-pot room temperature synthesis of Cu_2O/Ag composite nanospheres with enhanced visible-light-driven photocatalytic performance. Ind Eng Chem Res 53:16316–16323
51. Zhou LJ, Zou YC, Zhao J, Wang PP, Feng LL, Sun LW, Wang DJ, Li GD (2013) Facile synthesis of highly stable and porous Cu_2O/CuO cubes with enhanced gas sensing properties. Sensor Actuat B 188:533–539
52. Luo CC, Zhang YH, Zeng XW, Zeng YW, Wang YG (2005) The role of poly(ethylene glycol) in the formation of silver nanoparticles. J Colloid Interf Sci 288:444–448
53. Sun YG, Yin YD, Mayers BT, Herricks T, Xia YN (2002) Uniform silver nanowires synthesis by reducing $AgNO_3$ with ethylene glycol in the presence of seeds and poly(vinyl pyrrolidone). Chem Mater 14:4736–4745
54. Zhang DH, Liu XH (2013) Synthesis of polymer-stabilized monometallic Cu and bimetallic Cu/Ag nanoparticles and their surface-enhanced Raman scattering properties. J Mol Struct 1035:471–475
55. Feng LL, Zhang CL, Gao G, Cui DX (2012) Facile synthesis of hollow Cu_2O octahedral and spherical nanocrystals and their morphology-dependent photocatalytic properties. Nanoscale Res Lett 7:276
56. Xu HL, Wang WZ, Zhu W (2006) Shape evolution and size-controllable synthesis of Cu_2O octahedra and their morphology-dependent photocatalytic properties. J Phys Chem B 110:13829–13834
57. Zhou B, Wang HX, Liu ZG, Yang YQ, Huang XQ, Lü Z, Sui Y, Su WH (2011) Enhanced photocatalytic activity of flowerlike Cu_2O/Cu prepared using solvent-thermal route. Mater Chem Phys 126:847–852
58. Zhou B, Liu ZG, Zhang HJ, Wu Y (2014) One-pot synthesis of Cu_2O/Cu self-assembled hollow nanospheres with enhanced photocatalytic performance. J Nanomater 2014:291964
59. Bandara J, Guasaquillo I, Bowen P, Soare L, Jardim W, Kiwi J (2005) Photocatalytic storing of O_2 as H_2O_2 mediated by high surface area CuO. Evidence for a reductive-oxidative interfacial mechanism. Langmuir 21:8554–8559